TRANSMISSION ELECTRON MICROSCOPY EVIDENCE FOR EXPERIMENTAL ILLITIZATION OF SMECTITE IN K-ENRICHED SEAWATER SOLUTION AT 50ºC AND BASIC pH

A. Drief, F. Martinez-Ruiz, F. Nieto* and N. Velilla Sanchez

Departamento de Mineralogía y Petrología, Instituto Andaluz de Ciencias de la Tierra, Universidad de Granada-CSIC Av. Fuentenueva s/n, 18002 Granada, Spain

Abstract—Experimental illitization of smectite was studied by transmission electron microscopy (TEM) and X-ray diffraction (XRD). Experiments were performed on the <2 μm fraction consisting entirely of smectite separated from a soil formed on subvolcanic rock located in the External Zone of the Betic Cordilleras (southern Spain). Amounts of 0.25 g were added to different solutions: seawater, and three K-enriched seawater solutions prepared by adding KOH to seawater whose final [K] values were 0.1, 0.5 and 1 M, respectively. The experiments were performed at 50ºC over a period of 30 days. The XRD patterns showed no mineralogical changes in residues from seawater or from the 0.1 M [K] solution. With increasing pH and K molarity, the smectite peak, initially at 1.4 nm, became broader. This change in the smectite peak was more significant in the residue from the 1 M [K] solution. The appearance of a small shoulder at 1.0 nm in the residue from a 0.5 M [K] solution showed the beginning of illite formation. However, its appearance was clearer in XRD patterns of the residue corresponding to the 1 M [K] solution. The XRD data from air-dried, glycolated, and heated samples from the 1 M [K] solution indicated the presence of smectite, disordered interstratified illite-smectite (I-S) and illite.

   The TEM/AEM studies were performed on the residue corresponding to the 1 M [K] experiment. The HRTEM images revealed that smectite and illite occurred as separated packets with a ferroan lizardite, as a by-product of the smectite-to-illite reaction, interstratified and intergrown with illite. Smectite occurs both as 'rims' on the illite packet and in its core. The presence of smectite in the core of illite packet indicates that the lateral transition from smectite to illite was incomplete, taking place by direct replacement of smectite layers as a whole through a dissolution-precipitation mechanism. The experimental study shows that smectite may transform in a wide range of geological and artificial environments involving high-pH K-rich solutions.

 Key Words—AEM Analysis, Illite-Smectite, Intergrowth, Lizardite, Low Temperature, Potassium, Seawater.

INTRODUCTION

Smectite is one of the most abundant hydrous silicates produced by weathering and diagenetic processes. It plays an important role in environmental processes as an ion-absorption material, and its physical and chemical properties also make it suitable for industrial uses. Nevertheless, smectite can transform under natural conditions, converting to illite. The smectite to illite transformation mechanisms are some of the most intriguing questions in clay mineralogy and environmental science. Most of the progress in characterizing such mechanisms has been made in application to burial diagenesis. In general, during diagenesis, smectite is converted into illite as a response to depth (temperature) of burial with chemical exchange incorporating K and Al, and releasing water as well as other cations. A vast amount of research has been performed on the smectite to illite transformation in the burial diagenesis field (*e.g.* Nadeau *et al.*, 1985; Yau *et al.*, 1987; Ahn and Peacor, 1989; Hansen and Lindgreen, 1989; Inoue *et al.*, 1990; Buatier *et al.*, 1992; Nieto *et*

al., 1996; Clauer *et al.*, 1997). However, smectite transformation may take place in a wide range of natural environments other than during diagenetic processes, related (*e.g.* Cuadros and Linares, 1996) to its industrial applications. Smectite is used, for instance, in clay retaining barriers as a component of the buffer and backfill for waste disposal. Thus, the smectite to illite transformation is a key problem in this case because fluids may enter the clay barrier from concrete and significantly alter the pH and clay composition.

Because physical, mineralogical and chemical modifications affect the uses and industrial applications of smectite, special attention has been paid to experimental smectite transformation. The smectite to illite transformation has been investigated using natural smectite. The variables time, chemical composition and temperature have been widely varied. Whitney and Northrop (1988) studied the hydrothermal synthesis of R0 I-S from smectite at elevated temperature. Moore and Reynolds (1996) showed that the loss of expandability is, in general, a function of time and temperature. Cuadros and Linares (1996) used hydrothermal bentonite to study the kinetics of the smectite to illite transformation, in order to estimate the performance life of a bentonite barrier in

* E-mail address of corresponding author:
fnieto@ugr.es

a high-level nuclear waste repository. However, apart from temperature, time and composition, other factors also govern the extent of the smectite to illite transformation (Ahn *et al.*, 1988; Essene and Peacor, 1995). The most important additional factors are the water/rock ratio (Whitney, 1990), and the activity of interlayer cations, especially K concentration, which can significantly affect the rate of the smectite to illite transformation (Huang *et al.*, 1993). In fact, the effects of the solution chemistry at low temperature and high pH have been investigated in less detail than those at high temperature (Bauer and Velde, 1999). High-pH solution-mineral reactions, at low temperature, occur naturally in a variety of geological environments and engineered systems. The breakdown of concrete in natural environments releases Ca, Na and K into solution producing high-pH conditions (Andersson *et al.*, 1989; Lunden and Andersson, 1989). Several authors (*e.g.* Eberl *et al.*, 1993; Bauer and Velde, 1999) have investigated the effect of high molar KOH solutions on the mineralogy and solution chemistry during smectite degradation. However, the temperature used in their experiments was high (*e.g.* Bauer and Velde 1999).

Most experiments dealing with the smectite to illite transformation were carried out under hydrothermal conditions and less attention has been paid to low-temperature smectite transformation. The aim of this work was, therefore, to analyze, by means of HRTEM/AEM, the smectite-to-illite transformation at lower temperature than may be reached in a wide range of natural and artificial conditions, with a special focus on the effects of K concentration on the smectite-to-illite reaction. Because marine sediments are particularly abundant, seawater was selected as an experimental solution.

MATERIAL AND METHODS

Starting material

The experimental alteration was performed using a natural clastic smectite. Samples were taken from a soil derived from subvolcanic rocks in the External Zone of the Betic Cordilleras (southern Spain). This material was selected because in many natural environments smectite that transforms into illite during diagenesis is usually of clastic origin and, therefore, includes grains with a variety of chemical compositions. The smectite, here-after VS, was studied by Drief and Nieto (2000). X-ray diffraction and TEM analyses revealed a soil mineral composition similar to that of the parent rock, but containing a significant amount of smectite. No other layer silicate (*e.g.* illite, berthierine) was detected. The chemical composition of the VS smectite, determined by analytical electron microscopy (AEM), was reported by Drief and Nieto (2000) (Table 1). The VS smectite is 1*Md* polytype. This sample was selected because its interlayer composition was dominated by Ca and Na instead of K unlike the rest of the samples described by Drief and Nieto (2000).

Smectite treatment with K-enriched seawater solutions

The <2 μm fraction was separated from the VS soil by centrifugation and subsequent sedimentation, and then dried at room temperature. According to Drief and Nieto (2000), only smectite could be detected in this fraction. Smectite samples were ground smoothly in an agate mortar. Representative amounts of 0.25 g were added to different experimental solutions. These solutions were natural seawater, and three K-enriched solutions prepared by adding KOH to seawater whose final K molarity was 0.1, 0.5 and 1, respectively. The pH

Table 1. AEM analyses of the starting smectite using copper grids (1-11) and gold grids (12-15).

| | Structural formulae based on 11 oxygens Smectite from Drief and Nieto (2000) | | | | | | | | | | | | | | |
	1	2	3	4	5	6	7	8	9	10	11	12	13	14	15
Tetrahedral cations															
Si	3.23	3.86	3.74	3.81	3.74	3.70	3.45	3.69	3.69	3.43	3.62	3.27	3.11	3.16	3.84
^{IV}Al	0.77	0.14	0.26	0.19	0.26	0.30	0.55	0.31	0.31	0.57	0.38	0.73	0.89	0.84	0.16
Octahedral cations															
^{VI}Al	1.45	1.28	1.74	1.29	1.28	1.31	1.73	1.36	1.57	1.33	1.09	1.63	0.94	1.84	1.10
Mg	0.27	0.40	0.16	0.25	0.39	0.34	0.19	0.32	0.22	0.36	0.61	0.22	0.22	0.19	0.35
Fe	0.48	0.40	0.19	0.34	0.49	0.44	0.24	0.42	0.29	0.50	0.49	0.24	1.07	0.11	0.54
Σoct. cat.	2.19	2.07	2.09	2.15	2.16	2.09	2.16	2.10	2.08	2.19	2.19	2.10	2.24	2.13	1.99
Interlayer cations															
K	0.26	0.07	0.02	0.04	0.04	0.04	0.11	0.10	0.10	0.18	0.12	0.03	0.01	0.06	0.08
Ca	0.10	0.13	0.07	0.11	0.06	0.17	0.08	0.11	0.09	0.09	0.15	0.21	0.12	0.16	0.06
Na	0.00	0.00	0.00	0.00	0.00	0.00	0.00	0.00	0.00	0.00	0.00	0.23	0.16	0.25	0.10
Int. cha.	0.45	0.33	0.16	0.27	0.16	0.38	0.28	0.31	0.28	0.36	0.42	0.69	0.40	0.63	0.29

Σoct. cat. = sum of octahedral cations
Int. cha. = interlayer charge

of the solutions was 7.87 for starting seawater, and 10.35, 13.09 and 13.40 for the solutions with 0.1, 0.5 and 1 K molarity, respectively. The four experimental solutions were placed in glass flasks for 30 days with daily stirring. The entire experiment was carried out at 50ºC, which was judged to be high enough to allow reactions to occur without affecting mineral structures. Time and temperature were kept constant, whereas pH and K concentration were variable and the main focus of the experiment.

Examination of the material

X-ray diffraction. The starting material and the residual solid fraction from each solution after 30 days' reaction were smeared on glass slides and dried at room temperature. Three methods of preparation were used: (1) solvated with ethylene glycol at 80ºC for 24 h; (2) heated at 550ºC for 1 h; and (3) untreated. The XRD patterns were obtained using a Philips PW-1710 diffractometer using CuKα radiation (with graphite

Figure 1. XRD patterns of oriented untreated smectite and residues after 30 days' reaction with seawater and K-enriched seawater.

monochromator and automatic divergence slit) operating at 40 kV and 40 mA. The scanning speed was 2º2θ/min.

Electron microscopy. The solid residue from the 1 M [K] solution was selected for high-resolution transmission electron microscopy (HRTEM). The residue was embedded in epoxy resin and sectioned with a diamond knife (LKB ultramicrotome). The sections obtained (<50 nm thick) were deposited on carbon-coated copper grids. The TEM analyses were carried out using a Philips CM20 instrument equipped with an EDAX solid-state ultrathin-window EDX detector ('Centro de Instrumentacion Cientifica', Granada University). The acceleration voltage of the microscope was 200 kV and a lens aperture of 40 μm was used as a compromise between amplitude and phase contrast for the images. Reflections with *d*-values >0.4 nm were used for the lattice-fringe images. The AEM analyses were obtained only from thin edges in a scanning TEM (STEM) mode (<400 counts/s) using a 4 nm diameter beam and 20×100 nm scanning area. A low-background condenser aperture and an analytical Be sample holder were employed to improve spectrum quality. Muscovite, albite, biotite, spessartine, olivine and titanite were used to obtain k-factors to correct X-ray intensities by the thin-film method of Lorimer and Cliff (1976). Average errors for analyzed elements (two standard deviations), expressed as a percentage of the atomic proportions, are 6 (Na), 3 (Mg), 2 (Al), 4 (K), 4 (Ca), 5 (Ti), 3 (Mn) and 3 (Fe). A short counting time (30 s) was used because alkali loss was observed for long counting times (200 s). As usual in the literature, Fe was assumed to be Fe^{3+} for smectite-illite intergrowths and Fe^{2+} for ferroan lizardite-illite.

RESULTS

X-ray study

The XRD patterns from the <2 μm fraction of untreated sample from the VS soil and those from residues reacting with seawater and K-enriched seawater solutions are shown in Figure 1. Mineralogical changes were not observed in residues from seawater nor from the 0.1 M [K] solution. The smectite peak, initially at 1.4 nm, became broader with increasing K molarity. This change in the smectite peak was more significant in the residue from the 1 M [K] solution. Moreover, Figure 1 shows the appearance of a small shoulder at 1.0 nm in the residue from a 0.5 M [K] solution that became a well-defined peak in the residue corresponding to the 1 M [K] solution. The XRD data from air-dried, glycolated and heated samples from the 1 M [K] solution allowed us to distinguish among smectite, I-S interstratification and illite (Figure 2). When these samples were glycolated, the smectite peak shifted to 1.6 nm whereas the 1.0 nm peak remained unchanged. Furthermore, the second- and third-order basal reflections of smectite in Figure 2 are consistent with those
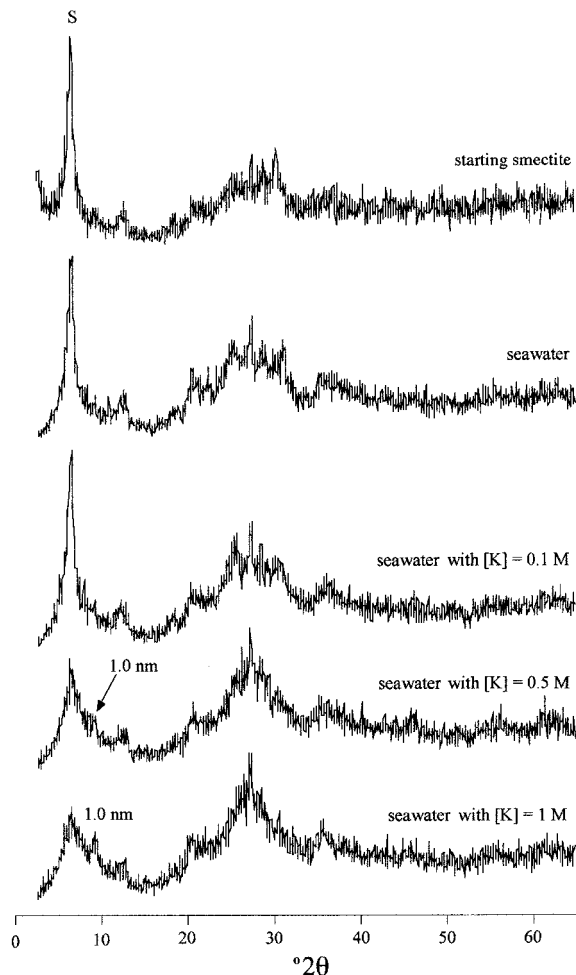
reported by Reynolds (1980) for randomly-interstratified I-S with a variable proportion of illite layers between 0 and 20%.

Electron microscopy

Transmission electron microscopy. The TEM images show smectite aggregates and typical morphologies of illite in the residue from the 1 M [K] solution (Figure 3). The smectite aggregates are formed by nano-sized spindle-like anastomosing particles, whereas illite particles show a platy, elongate shape characteristic of illite. The HRTEM images show packets of illite intergrown with smectite after 30 days' reaction in the 1 M [K] solution (Figure 4a). The selected area electron diffraction (SAED) patterns of illite packets in Figure 4a show 1.0 nm periodicity (Figure 4b). Figure 4c shows two packets with distinct types of 1.0 nm layers that are clearly distinguished. The upper packet, designated as S,

consists of imperfect and curved layers having a spacing ranging from 1.0 to 1.2 nm, and the lower packet, designated as I, consists of straight, well-defined and defect-free 1.0 nm layers. The S packet type is less abundant in the stack of layers shown in Figure 4a, and occurs as a rim on the illite particle, whereas the I type comprises most of the packet. The wavy layers having 1.0 – 1.2 nm spacing were interpreted as smectite, whereas the straight layers were interpreted as illite on the basis of textural and chemical data (see below). However, some smectite layers could have collapsed under the TEM vacuum and thus be misinterpreted as illite layers. Figure 4c reveals relationships that imply a lateral transition of smectite to illite. In fact, the illite packet contains smectite-like layers (those labeled with S inside the illite packet in Figure 4c) that exhibit the same textural characteristics as the 1.0 – 1.2 nm layer type discussed above. These data reveal that the smectite to illite transformation occurs simultaneously over whole packets and not layer-by-layer with passing time through the formation of I-S mixed-layers. In addition, no I-S mixed-layering was detected. The only intermediate products of transformation found in the samples correspond to intergrowths of illite and smectite packets. Nevertheless, as mentioned before, it is possible that some illite packets could contain minor smectite layers collapsed to 1 nm. The analysis of electron diffraction patterns of illite particles (Figure 5a) shows that they are characterized by sharp, intense reflections and by 2.0 nm periodicity in both lattice fringes and SAED patterns (Figure 5b). The presence of the 2*M* polytype as a direct product of smectite transformation is consistent with the results obtained by Dong and Peacor (1996). The intensity and sharpness of the spots were coherent with the lattice-fringe perfection.

The TEM images also show the presence of irregularly mixed-layer 0.7 and 1.0 nm phases (Figure 6a), where only discrete 0.7 nm layers were observed. Because 1.0 nm layers are dominant, the SAED patterns show only 1.0 nm periodicity
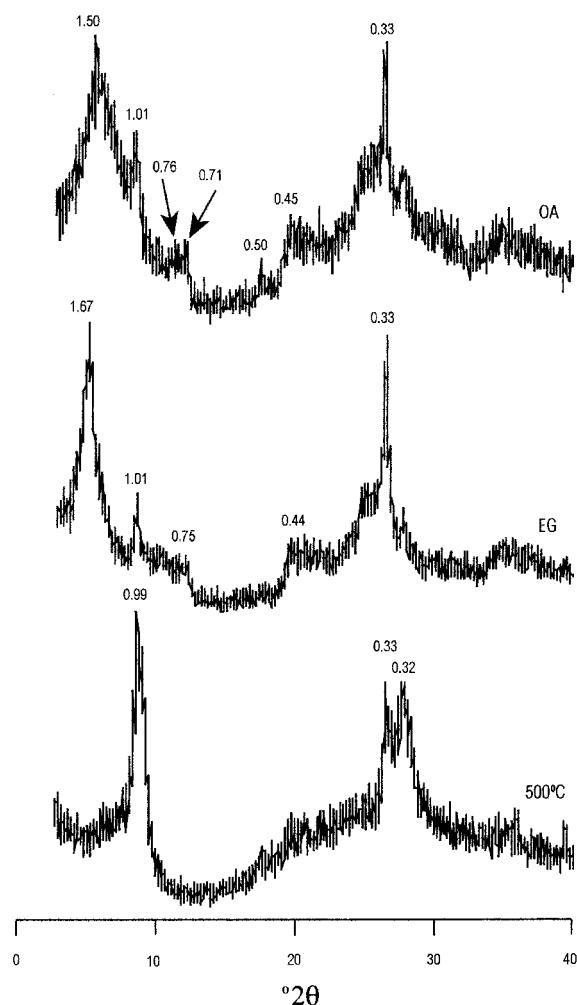

Figure 2. XRD patterns of the oriented residue corresponding to the experiment performed with 1 M K seawater solution. OA = oriented aggregate, EG = treatment with ethylene glycol, and 500°C = heated at 500°C. Spacings in nm.
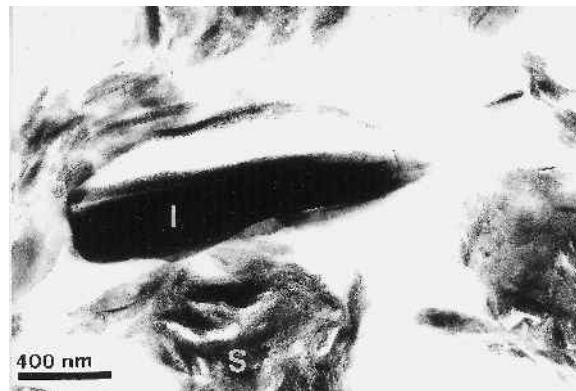

Figure 3. TEM image of a typical morphology of illite (I) and smectite aggregates (S) after 30 days' reaction with 1 M K solution.
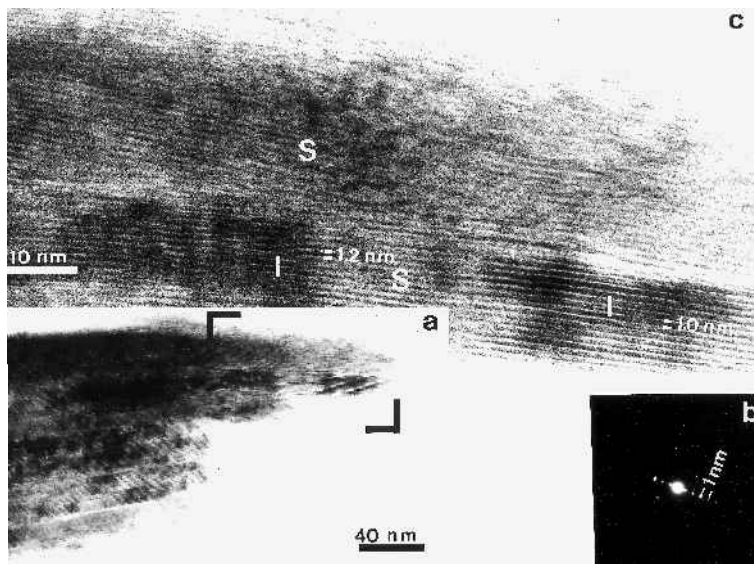
Figure 4. TEM image of illite particle; (b) electron diffraction patterns of the illite particle shown in (a); and (c) HRTEM image of the zone indicated in (a). I = illite layers and S = smectite layers.

(Figure 6b). Nevertheless, some spreading of the (00*l*) reflections along the *c** could have been a result of a disorder in periodicity caused by individual 0.7 nm layers. The 1.0 nm and 0.7 nm layers also occur as separate and discrete packets labeled I and L, respectively, in Figure 7. The packets of 1.0 nm layers exhibit both wavy (domain S in Figure 7) and straight (domain I in Figure 7) layers, as discussed above for intergrowths of smectite and illite packets.

Analytical electron microscopy. Chemical analyses of pure or almost pure illite were obtained from areas with SAED patterns similar to those in Figure 5b. The AEM data normalized to 11 O are listed in Table 2. Calcium is

an abundant interlayer cation in the starting smectite (Drief and Nieto, 2000), though it is completely absent in illite (Table 2), whereas K is, in general, the only interlayer cation present, with the exception of some uncommon spots where Na was also detected (Table 2). The Si:Al ratio is quite similar in all the analyses and ranges from 1.02 to 1.19. The structural illite formulae reported here are consistent with those of typical illites formed during diagenetic processes (*e.g.* Środoń *et al.*, 1986; Nieto *et al.*, 1996). The illite obtained has a slightly phengitic composition, with Mg > Fe (Mg $\leqslant$ 0.23/11 O). Also, structural formulae from intergrowths of smectite and illite packets were calculated from AEM data on the basis of 11 O (Table 2). The analyses obtained provide intermediate compositions between smectite and illite, K being the dominant interlayer
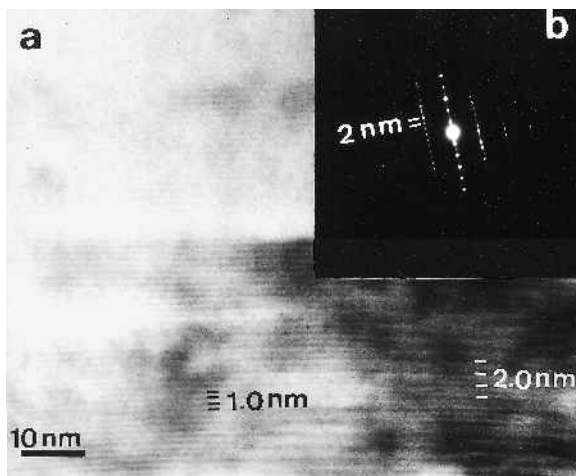

Figure 5. (a) HRTEM image of an illite particle formed in 1 M K solution showing 1- and 2-layer stacking; and (b) electron diffraction patterns of the particle shown in (a) seen from the <110> direction.
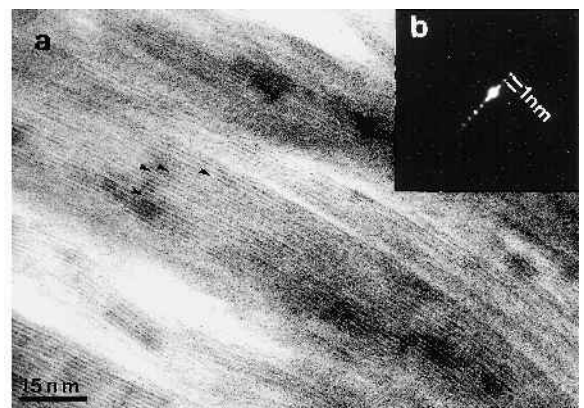

Figure 6. (a) HRTEM image of 0.7–1.0 nm interstratification formed in 1 M K solution; arrows indicate individual 0.7 nm layers; and (b) electron diffraction patterns of the particle shown in (a).
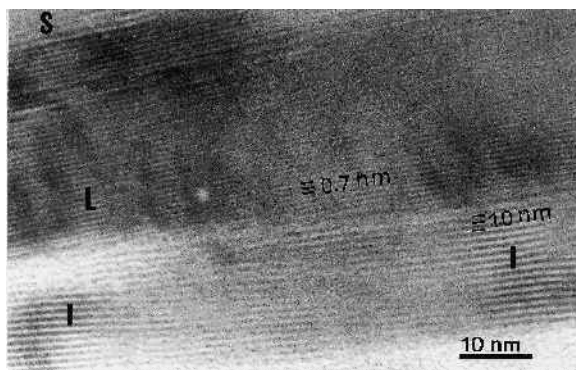
Figure 7. HRTEM images of 0.7 and 1.0 nm intergrowths. I = illite, L = ferroan lizardite (see discussion for explanation), and S = smectite.

cation. As for illite, Na was only detected in few spots but Ca was absent. In addition, octahedral sheets have also an intermediate composition between those of smectite and illite.

Data from smectite, intergrowths of smectite and illite packets, and illite compositions reveal significant trends (Figure 8). The plot of Si *vs.* K shows a negative correlation for the two elements (Figure 8a). In contrast, the plot of Al *vs.* K shows a positive correlation (Figure 8b). The plot of ^{VI}Al *vs.* K shows that octahedral Al is correlated positively with K (Figure 8c). The increase in K and the relative decrease in Na and Ca shown by the plot of K/(K+Na+Ca) *vs.* (K+Na+Ca) (Figure 8d) reflect the progress in the illitization process. However, the most striking feature in the interlayer composition is that the maximum value of the K/(K+Na+Ca) ratio (=1) was reached in the intergrowths of smectite and illite packets before complete illitization. The decrease in Si in the tetrahedral sheet during the smectite to illite transformation was accompanied by an increase in Al in both tetrahedral and octahedral sheets and a concomitant fixation of K in the

interlayer site. Octahedral Al substitutions for Fe and Mg are negatively correlated (Figure 8e,f).

We were not able to obtain pure chemical analyses of the 0.7 nm phase as it was a minor phase and always intergrown with a 1.0 nm phase in areas too small to be resolved by AEM. However, chemical data in Table 3, obtained in areas similar to those shown in Figure 7, show compositions typical of a di-trioctahedral layer silicate (*e.g.* illite-7 Å mixed-layer phase). The structural formulae reported in Table 3, performed on 0.7–1.0 nm intergrowths, were calculated from AEM analyses on the basis of 11 O in order to characterize the chemical composition of the 0.7–1.0 nm intergrowths. Potassium was the dominant interlayer cation, suggesting that significant amounts of illite are present. The Na was absent in all the areas analyzed. Although some analyses showed a small amount of Ca, this cation was generally absent. Its presence, however, suggests that smectite is also intergrown with illite. The octahedral composition was dominated by Fe, Mg and Al, in decreasing order.

DISCUSSION

Smectite to illite transformation

The results obtained from this study further demonstrate the effect of K concentration and pH on the smectite to illite transformation, which involves chemical changes in tetrahedral and octahedral sheets as well as in the interlayer cations. The low Si:Al ratio in illite emphasizes the importance of the increase in Al content during the smectite to illite transformation, which was accompanied by the release of Fe, Mg and Si. However, the most significant change in composition during the experimental alteration was the increase in K in the interlayer site with a concomitant decrease in Na and Ca.

The XRD patterns showed that the increasing K concentration made the smectite peak broader. The TEM images revealed that illite and smectite occur as distinct

Table 2. AEM analyses of illite and I-S intergrowths formed at 30 days of reaction in 1 M [K] seawater solution.

	Structural formulae based on 11 oxygens													
	Illite								I-S intergrowth areas					
	1	2	3	4	5	6	7	8*	1	2	3	4	5	6	7
Tetrahedral cations														
Si	3.12	3.08	3.08	3.12	3.08	3.12	2.95	3.14	3.50	3.27	3.69	3.55	3.54	3.58	3.23
^{IV}Al	0.88	0.92	0.92	0.88	0.92	0.88	1.05	0.86	0.50	0.73	0.31	0.45	0.46	0.42	0.77
Octahedral cations														
^{VI}Al	1.97	1.97	1.97	1.90	1.84	1.74	1.86	1.84	1.95	2.03	1.66	1.67	1.74	1.74	1.79
Mg	0.11	0.16	0.15	0.22	0.13	0.23	0.10	0.12	0.05	0.08	0.16	0.16	0.17	0.25	0.14
Fe	0.04	0.03	0.03	0.06	0.13	0.18	0.14	0.11	0.11	0.05	0.33	0.24	0.19	0.18	0.24
Σoct. cat.	2.12	2.16	2.15	2.17	2.10	2.14	2.10	2.18	2.10	2.16	2.15	2.07	2.10	2.17	2.16
Interlayer cations														
K	0.67	0.64	0.64	0.63	0.65	0.63	0.82	0.84	0.35	0.40	0.36	0.45	0.51	0.32	0.43
Na	0.00	0.00	0.00	0.00	0.23	0.23	0.18	0.00	0.00	0.00	0.00	0.18	0.00	0.00	0.23
Int. cha.	0.67	0.64	0.64	0.63	0.88	0.86	1.00	0.84	0.35	0.40	0.36	0.63	0.51	0.32	0.66

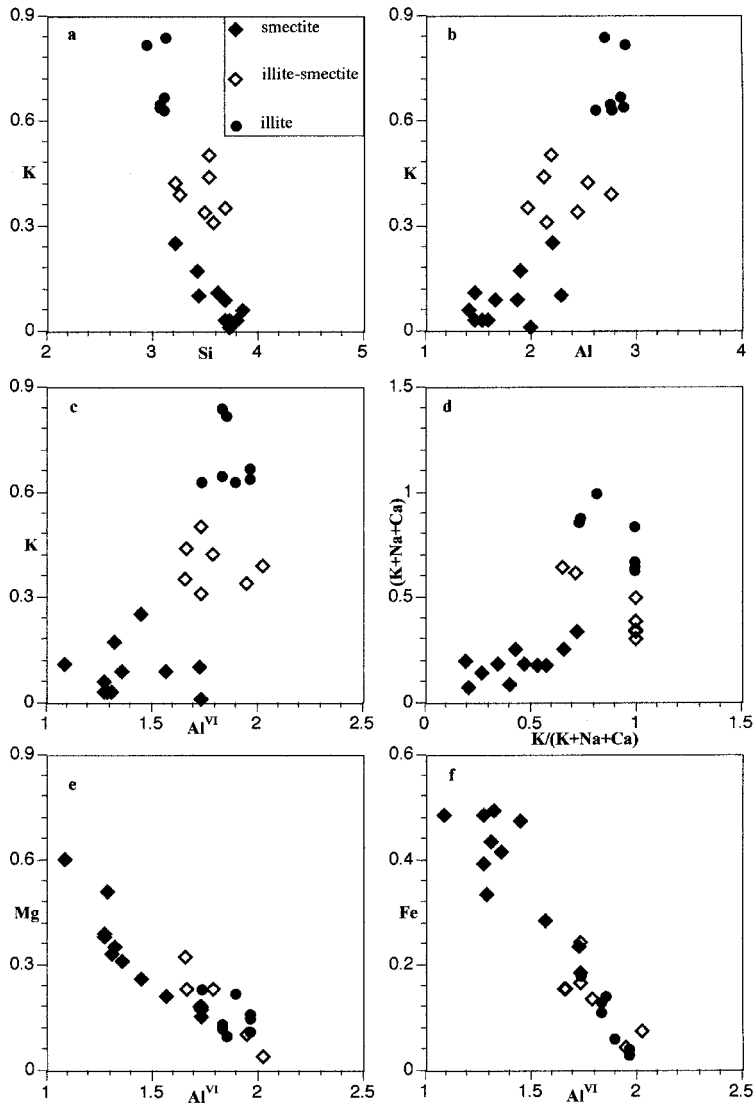Σoct. cat. = sum of octahedral cations, Int. cha. = interlayer charge. * = analysis with traces of Ti

Figure 8. Selected binary diagrams showing the evolution of the chemical composition of smectite to illite through I-S intergrowths.

and discrete packets of layers. Such intergrowths of illite and smectite packets could limit (or decrease) the effective smectite crystallite thickness for diffraction and therefore increase the incoherent X-ray scattering effect on smectite to result in a broadening of reflections. In addition, the XRD study showed that the smectite intergrown with illite corresponds, in fact, to interstratified I-S with up to 20% illite. The broadness of the smectite peaks (second and third order, in Figure 2) after treatment with ethylene glycol is related to a wide variation in the proportion of illite layers interstratified with the smectite. Between 0 and 20% of illite layers are randomly interstratified with smectite as R0 I-S. However, according to Kim *et al.* (1995) and Dong *et al.* (1997), the so-called randomly mixed-layer I-S, determined by the XRD method, could have been misinterpreted in the past. Furthermore, the intergrowths of smectite and illite packets in Figure 8 show that many

analyses contain only K in their interlayer sites. This fact indicates that smectite became K rich before transforming to illite.

Two broad categories of reaction mechanism for smectite–illite transformation have been established: (1) solid-state mechanisms which involve gradual replacement of the parent mineral (smectite) by the daughter mineral (illite) in close topotactic contact (Altaner and Ylagan, 1997). Such a model, which typically also involves fluids that can act as catalysts and transport media (Veblen, 1992), is sometimes referred to as a "layer-by-layer transformation"; (2) dissolution-crystallization mechanisms which involve complete dissolution of the parent mineral followed by nucleation and growth of the daughter mineral as a separate or epitaxial grain (Altaner and Ylagan, 1997). In such a model, the memory of the parent mineral is lost. Features of this mechanism are changes in polytype and loss of

Table 3. AEM analyses based on 11 oxygens of the 0.7–10 nm intergrowths formed at 30 days' reaction in 1 M [K] seawater solution.

	Structural formulae based on 11 oxygens										
	1	2	3	4	5	6	7	8	9	10*	11*
Tetrahedral cations											
Si	3.17	3.10	3.13	3.17	3.36	2.98	3.27	3.25	3.19	3.11	3.09
^{IV}Al	0.83	0.90	0.87	0.83	0.64	1.02	0.73	0.75	0.81	0.89	0.91
Octahedral cations											
^{VI}Al	0.92	0.43	0.40	0.46	0.48	0.13	0.48	0.28	0.97	0.13	0.16
Mg	0.50	1.22	1.23	1.22	1.00	1.56	1.18	1.15	0.29	0.47	0.45
Fe	1.25	1.28	1.30	1.28	1.36	1.45	1.25	1.45	1.31	2.20	2.17
Σoct. cat.	2.68	2.94	2.93	2.95	2.84	3.14	2.91	2.88	2.56	2.80	2.78
Interlayer cations											
Ca	0.02	0.02	0.00	0.02	0.04	0.04	0.03	0.04	0.08	0.00	0.00
K	0.51	0.55	0.61	0.44	0.40	0.53	0.39	0.62	0.41	0.83	0.90
Int. cha.	0.55	0.59	0.61	0.47	0.48	0.60	0.44	0.70	0.57	0.83	0.90

Σoct. cat. = sum of octahedral cations, Int. cha. = interlayer charge, * = analysis with traces of Ti

morphological characteristics of the parent mineral. There is still considerable controversy as to which reaction mechanism applies to illitization in natural systems. However, several studies emphasize that different mechanisms apply in different geological environments. The smectite–illite reaction in the present study does not occur through mixed-layer I-S and the presence of smectite in the core of illite domains (Figure 4c) indicates that the lateral transition from smectite to illite was incomplete. This observation suggests that illite formation takes place by replacement of layers of the original smectite as a whole and not layer-by-layer. Furthermore, the parent and daughter minerals exhibit different morphological and crystal-chemical characteristics (smectite *vs.* illite and a 0.7 nm trioctahedral phase). These minerals occur as separated packets (Figure 7). The reactant (smectite) and products (illite and 0.7 nm phase) are different not only in the interlayer sites but also in the octahedral and tetrahedral sheets. These observations imply a disappearance of the parent mineral and a further precipitation of new phases by dissolution-precipitation mechanism.

Formation of ferroan lizardite

In the present study, chemical analyses of the 0.7–1.0 nm intergrowths, similar to those in Figure 7, ranged between ferroan lizardite as reported by Drief *et al.* (2001) and illite or intergrowths of smectite and illite packets (Figure 9). Drief *et al.* (2001) identified ferroan lizardite as a product of experimental alteration of a subvolcanic rock under given chemical conditions. They could easily distinguish ferroan lizardite from berthierine obtained under different experimental conditions, because of their very different Si:Al ratios (see Figure 9). Chloritic clays, as by-products of the reaction, have an independent role in the development of mica as by-product. The 1.4- and 0.7 nm layers, related to smectite–illite transformation, were observed by several authors (*e.g.* Li *et al.*, 1997). However, due to their

occurrence interstratified or intergrown with illite, few chemical compositional data were reported. This is the first time that ferroan lizardite has been reported as a by-product of the smectite–illite reaction. Therefore, 0.7 nm phases that occur together with illite during the smectite–illite transformation might sometimes be ferroan lizardite instead of berthierine.

The chemistry and occurrence of these minerals may be fundamental in explaining the reaction of smectite breakdown to illite. Drief and Nieto (2000) suggested a tentative reaction for the origin of both illite and chlorite from a typical composition of clastic-sediment-forming smectite. The reaction suggested is consistent with the data of the present study. In fact, our results show the presence of ferroan lizardite (Figure 7), which could behave as a sink for Fe and Mg released by smectite. Hower *et al.* (1976) detected the development of chlorite related to the smectite to illite transformation. Subsequently, detailed chemical analyses and TEM
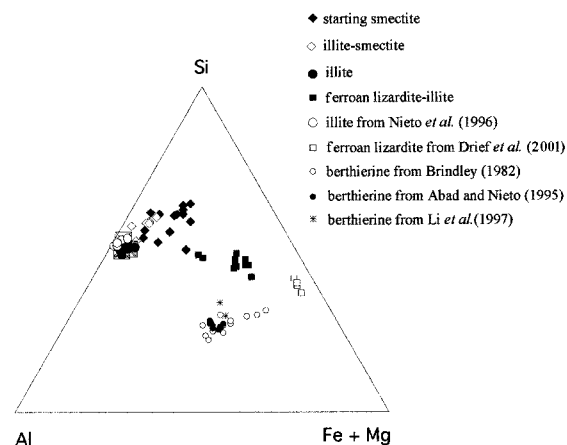

Figure 9. Plot of chemical composition in the Si-Al-(Fe+Mg) ternary system of the 1 M K solution products along with illite, ferroan lizardite and berthierine reported previously in the literature.

investigations indicated the development of chlorite from smectite, along with the transformation of smectite to illite (Curtis, 1985; Ahn and Peacor, 1985). Since berthierine is chemically similar to Fe-rich chlorite, it was considered by many authors to be a precursor of chlorite during diagenesis (*e.g.* Longstaffe *et al.*, 1992). In fact, chlorite-berthierine intergrowths have also been described by Jiang *et al.* (1992). Nevertheless, the presence of ferroan lizardite as a precursor of chlorite has not been reported so far. The present experimental study showed the formation of ferroan lizardite as a by-product of the smectite–illite transformation that could also exist in natural environments as a precursor of chlorite during diagenetic processes.

K availability and pH

Most of the models proposed to explain the smectite to illite transformation consider K availability for such a transformation, the origin of which in natural environments has been assigned to feldspars and/or mica (*e.g.* Hower *et al.*, 1976; Kirsimäe *et al.*, 1999). Huang *et al.* (1993) experimentally quantified the kinetics of smectite to illite conversion concluding that temperature, time and K are by far the most important parameters controlling this conversion in hydrothermal systems. The same authors derived an empirical kinetic model which demonstrated that K concentration in pore-fluids enhanced the illitization of Wyoming bentonite and that the variation of K in shale pore-fluids can significantly affect the rate of smectite to illite transformation. In the same way, Li *et al.* (1995) showed that authigenetic clays in shales of the Precambrian (1.1 Ga) Nonesuch Formation in the vicinity of White Pine Copper mine, Michigan, were still I-S mixed layers mostly due to the lack of K availability.

On the other hand, smectites having K as the dominant interlayer cation have recently been reported as occurring in many sites, including Gulf Coast mudstones (Freed and Peacor, 1992), Barbados accretionary wedge bentonites (Buatier *et al.*, 1992), altered mid-oceanic-ridge basalt (Shau and Peacor, 1992), marine muds from the Mississippi Delta (Hover *et al.*, 1995), Nankai Trough bentonites (Masuda *et al.*, 1996), and bentonite and associated sediments from Kaka Point, New Zealand (Li *et al.*, 1997). Drief and Nieto (2000) also found that significant amounts of K concentrated in the interlayer sites of clastic-sediment-forming smectites before undergoing diagenesis. They showed that the K enrichment of smectite necessary to produce illite during diagenesis may be less than that previously assumed in the literature and, therefore, an external supply of K may not be an absolutely necessary condition for the development of mature micas. In the light of these observations from the literature, it is inferred that the intrinsic or extrinsic supply of K is necessary for the development of mature mica. In fact, in this experiment, illite was clearly identified by XRD only when it formed

in the 1 M solution, since K-poor smectite was selected for this experiment.

The increase in K molarity during this experiment was associated with increasing pH solution that could have also enhanced the smectite–illite transformation. The use of KCl instead of KOH solution would have decreased the reaction rate significantly (*e.g.* Cuadros and Linares, 1996). Both K^+ and H^+ ions are crucial for the development of mica from smectite. The present experimental work demonstrates, therefore, that smectite may transform in a wide range of geological environments involving K-enriched fluids. These, associated with high-pH conditions, also occur in a variety of engineered systems, such as radioactive waste disposal, and could significantly alter the original smectite.

CONCLUSIONS

The results obtained from this study demonstrate that both K and pH are crucial for the development of mica from smectite. The intrinsic or extrinsic supply of K is necessary for the development of mature mica. In fact, in this experiment, illite was clearly identified by XRD only when it formed in the 1 M solution. The presence of smectite in the core of illite domains suggests that this forms by replacement of layers of the original smectite as a whole through a dissolution-precipitation mechanism and not layer by layer. In the present experiment, ferroan lizardite was reported for the first time as a by-product of the smectite–illite reaction. Therefore, the 0.7 nm phases that occur along with illite during the smectite–illite transformation might sometimes be ferroan lizardite instead of berthierine.

ACKNOWLEDGMENTS

REFERENCES

Abad-Ortega, M.M. and Nieto, F. (1995) Genetic and chemical relationships between berthierine, chlorite and cordierite in nodules associated to granitic pegmatites of Sierra Albarrana (Iberian Massif, Spain). *Contributions to Mineralogy and Petrology*, **120**, 327–336.

Ahn, J.H. and Peacor, D.R. (1985) Transmission electron microscopic study of diagenetic chlorite in Gulf Coast argillaceous sediments. *Clays and Clay Minerals,* **33**, 228–236.

Ahn, J.H. and Peacor, D.R. (1989) Illite/smectite from Gulf Coast shales: a reappraisal of transmission electron microscope images. *Clays and Clay Minerals*, **37**, 542–546

Ahn, J.H., Peacor, D.R. and Coombs, D.S. (1988) Formation mechanisms of illite, chlorite and mixed layer illite-chlorite in Triassic volcanogenic sediments from the Southland Syncline, New Zealand. *Contributions to Mineralogy and Petrology*, **99**, 82–89.

Altaner, S.P. and Ylagan, R.F. (1997) Comparison of structural models of mixed-layer illite-smectite and reaction mechanisms of smectite illitization *Clays and Clay Minerals*, **45**, 517–533.

Andersson, K., Allard, B., Bengtsson, M. and Magnusson, B. (1989) Chemical composition of cement pore waters. *Cement and Concrete Research*, **19**, 327–332.

Bauer, A. and Velde, B. (1999) Smectite transformation in high molar KOH solutions. *Clay Minerals*, **34**, 259–273.

Brindley, G.W. (1982) Chemical compositions of berthierines. A review. *Clays and Clay Minerals*, **30**, 153–155.

Buatier, M., Peacor, D.R. and O'Neil, J.R. (1992) Smectite-illite transition in Barbados accretionary wedge sediments: TEM and AEM evidence for a dissolution/crystallization origin at low temperature. *Clays and Clay Minerals*, **40**, 65–80.

Clauer, N., Środoń, J., Francu, J. and Šucha, V. (1997) K-Ar dating of illite fundamental particles separated from illite-smectite. *Clay Minerals*, **32**, 181–196.

Cuadros, J. and Linares, J. (1996) Experimental kinetic study of the smectite-to-illite transformation. *Geochimica et Cosmochimica Acta*, **60**, 439–453.

Curtis, C.D. (1985) Clay mineral precipitation and transformation during burial diagenesis. *Philosophical Transactions of the Royal Society of London*, **A 315**, 91–105.

Dong, H. and Peacor, D.R. (1996) TEM observations of coherent stacking relations in smectite, I/S and illite of shales: evidence for MacEwan crystallites and dominance of 2M1 polytypism. *Clays and Clay Minerals*, **44**, 257–275.

Dong, H., Peacor, D.R. and Freed, R.L. (1997) Phase-relations among smectite, R1 illite-smectite, and illite. *American Mineralogist*, **82**, 379–391.

Drief, A. and Nieto, F. (2000) Chemical composition of smectites formed in clastic sediments. Implications for the smectite-illite transformation. *Clay Minerals*, **35**, 665–678.

Drief, A., Nieto, F. and Sánchez-Navas, A. (2001) Experimental clay-mineral formation from a subvolcanic rock by interaction with 1 M NaOH solution at room temperature. *Clays and Clay Minerals*, **49**, 92–106.

Eberl, D.D., Velde, B. and McCormick, T. (1993) Synthesis of illite-smectite from smectite at earth surface temperatures and high pH. *Clay Minerals*, **28**, 49–60.

Essene, E.J. and Peacor, D.R. (1995) Clay mineral thermometry: A critical perspective. *Clays and Clay Minerals*, **43**, 540–553.

Freed, R.L. and Peacor, D.R. (1992) Diagenesis and the formation of authigenic illite-rich I/S crystals in the Gulf Coast shales: TEM study of clay separates. *Journal of Sedimentology and Petrology*, **62**, 220–234.

Hansen, P.L. and Lindgreen, H. (1989) Mixed-layer illite/smectite diagenesis in Upper Jurassic claystones from the north Sea and onshore Denmark. *Clay Minerals*, **24**, 197–213.

Hover, V.C., Walter, L.M., Peacor, D.R. and Martini, A.M. (1995) K-uptake by smectite during early marine diagenesis in brackish and hypersaline depositional environments (abstract). *32nd Clay Minerals Society Annual Meeting Program and Abstracts*, p. 61.

Hower, J., Eslinger, E.V., Hower, M.E. and Perry, E.A. (1976) Mechanism of burial metamorphism of argillaceous sediments: 1. Mineralogical and chemical evidence. *Geological Society of American Bulletin*, **87**, 725–737.

Huang, W.-L., Longo, J.M. and Pevear, D.R. (1993) An experimentally derived kinetic model for smectite-to-illite conversion and its use as a geothermometer. *Clays and Clay Minerals*, **41**, 162–177.

Inoue, A., Watanabe, T., Kohyama, N. and Brusewitz, A.M. (1990) Characterization of illitization of smectite in bentonite beds at Kinekulle, Sweden. *Clays and Clay Minerals*, **38**, 241–249.

Jiang, W.T., Peacor, D.R. and Slack, J.F. (1992) Microstructures, mixed layering, and polymorphism of chlorites and retrograde berthierine in the Kidd Creek Massive sulfide deposits, Ontario. *Clays and Clay Minerals*, **40**, 501–514.

Kim, J.W., Peacor, D.R., Tessier, D. and Elsass, F. (1995) A technique for maintaining texture and permanent expansion of smectite interlayers for TEM observations. *Clays and Clay Minerals*, **43**, 51–57.

Kirsimäe, K., Jørgensen, P. and Kalm, V. (1999) Low-temperature diagenetic illite-smectite in Lower Cambrian clays in North Estonia. *Clay Minerals*, **34**, 151–163.

Li, G., Mauk, J.L. and Peacor, D.R. (1995) Preservation of clay minerals in the Precambrian (1.1 Ga) Nonesuch Formation in the vicinity of the White Pine copper mine, Michigan. *Clays and Clay Minerals*, **43**, 361–376.

Li, G., Donald, R., Peacor, D.R. and Coombs, D.S. (1997) Transformation of smectite to illite in bentonite and associated sediments from Kaka Point, New Zealand: Contrast in rate and mechanism. *Clays and Clay Minerals*, **45**, 54–67.

Longstaffe, F.J., Racki, M.A. and Ayalon, A. (1992) Stable isotope studies of diagenesis in berthierine-bearing oil sands, Clearwater Formation, Alberta. Pp. 955–958 in: *Water Rock Interaction, Moderate and High Temperature Environments*. Proceeding of the Seventh International Symposium on Water-Rock interaction volume **2** (Y.K. Kharaka and A.S. Maest, editors). A.A. Balkema, Rotterdam, The Netherlands.

Lorimer, G.W. and Cliff, G. (1976) Analytical electron microscopy of minerals. Pp. 506-519 in: *Electron Microscopy in Mineralogy* (H.R. Wenk, editor). Springer-Verlag, New York.

Lunden, I. and Andersson, K. (1989) Modeling the mixing of cement pore water and groundwater using the PHREEQE code. *Materials Research Society Symposium Proceedings*, **127**, 949–956.

Masuda, H., O'Neil, J.R., Jiang, W.-T. and Peacor, D.R. (1996) Relation between interlayer composition of authigenic smectite, mineral assemblages, I/S reaction rates and fluid composition in silicic ash of the Nankai Trough. *Clays and Clay Minerals*, **44**, 443–459.

Moore, D.M. and Reynolds, C.R., Jr. (1996) *X-ray Diffraction and the Identification and Analysis of Clay Minerals*. Oxford University Press, New York.

Nadeau, P.H., Farmer V.C., McHardy, W.J. and Bain, D.C. (1985) Compositional variations of the Unterrupsroth Beidellite. *American Mineralogist*, **70**, 1004–1010.

Nieto, F., Ortega-Huertas, M., Peacor, D.R. and Arostegui, J. (1996) Evolution of illite/smectite from early diagenesis through incipient metamorphism in sediments of the Basque-Cantabrian Basin. *Clays and Clay Minerals*, **44**, 304–323.

Reynolds, R.C. (1980) Interstratified Clay Minerals. Pp. 249–303 in: *Crystal Structure of Clay Minerals and their X-ray Identification* (G.W. Brindley and G. Brown, editors). Monograph **5**, Mineralogical Society, London.

Shau, Y.-H. and Peacor, D.R. (1992) Phyllosilicates in hydrothermally altered basalts from DSDP Hole 504B, Leg 83-A TEM and AEM study. *Contributions to Mineralogy*

and Petrology, **112**, 119–133.

Środoń, J., Morgan, D.J., Eslinger, E.V., Eberl, D.D. and Karlinger, M.R. (1986) Chemistry of illite/smectite and end-member illite. *Clays and Clay Minerals,* **34**, 368–378.

Veblen, D.R. (1992) Electron microscopy applied to non-stochiometry, polysomatism, and replacement reactions in minerals. Pp. 181–229 in: *Minerals and Reactions at the Atomic Scale: Transmission Electron Microscopy* (P.R. Buseck, editor). Reviews in Mineralogy, **27**. Mineralogical Society of America, Washington, D.C.

Whitney, G. (1990) Role of water in the smectite to illite reaction. *Clays and Clay Minerals*, **38**, 343–350.

Whitney, G. and Northrop, H.R. (1988) Experimental investigation of the smectite to illite reaction: dual reaction mechanisms and oxygen isotope systematics. *American Mineralogist*, **73**, 77–90.

Yau, Y.-C., Peacor, D.R., Essene, E.J., Lee, J.H., Kuo, L.C. and Cosca, M.A. (1987) Hydrothermal treatment of smectite, illite, and basalt to 460°C: Comparison of natural with hydrothermally formed clay minerals. *Clays and Clay Minerals,* **35**, 241–250.